OPEN ACCESS
Journal of Multidisciplinary Applied Natural Science Vol. 6 No. 2 (2026) https://doi.org/10.47352/jmans.2774-3047.375
Check for updates
Research Article

New Pyrrole-Chalcone Hybrids Against Acetylcholinesterase: Synthesis, *In Vitro*, and Computational Studies

Dadan Ridwanuloh, Ade Danova, Elvira Hermawati, Warinthorn Chavasiri, Ihsanawati Ihsanawati, and Anita Alni*

Received : August 8, 2025	Revised : December 12, 2025	Accepted : February 10, 2026	Online : March 20, 2026

Abstract
Acetylcholinesterase (AChE) inhibition remains a central therapeutic approach for Alzheimer's disease (AD), as it helps preserve synaptic acetylcholine levels, enhances cholinergic neurotransmission, and mitigates early cognitive decline. In this study, eight novel pyrrole–chalcone hybrids (**3–10**), consisting of four pyrrole–chalcones (**3–6**) and four pyrrole–chalcone amides (**7–10**), were designed, synthesized, and biologically evaluated for AChE inhibition. Among them, compound **8** (*N*-(4-methoxybenzyl)-pyrrole–chalcone amide) and compound **10** (*N*-(3,4-dimethoxybenzyl)-pyrrole–chalcone amide) demonstrated the strongest inhibitory activity, with IC_{50} values of 3.1 and 2.8 µM, respectively, comparable to galantamine. Kinetic assays confirmed that both compounds act as noncompetitive inhibitors, as indicated by reduced V_{max} without significant alteration in K_m, while compound **10** exhibited K_i of 0.8 µM, reflecting high enzyme affinity. Molecular docking revealed strong binding interactions of compounds **8** and **10** with key AChE residues (Trp84, Phe330, Tyr334), supported by *π–π* stacking, *π–alkyl* interactions, and hydrogen bonding, with binding energies of –9.2 (compound **8**) and –8.9 kcal/mol (compound **10**). Molecular dynamics simulations further demonstrated that compound **10** forms a more stable and compact complex with AChE, as indicated by consistent RMSD values and a stable radius of gyration. SwissADME analysis confirmed favorable pharmacokinetic profiles for both ligands, including Lipinski compliance, high GI absorption, and absence of PAINS alerts, despite the lack of predicted BBB permeability. Overall, compound **10** emerges as the most promising noncompetitive AChE inhibitor in this series, exhibiting strong binding affinity, structural stability, and drug-likeness, thus warranting further optimization and *in vivo* evaluation.

Keywords: acetylcholinesterase inhibitors, Alzheimer's disease, noncompetitive inhibition, pyrrole–chalcone hybrids

1. INTRODUCTION

Progressive memory loss and general cognitive decline are indications of Alzheimer's disease (AD), a genetically complicated, progressive, and irreversible neurodegenerative disease of the brain. Although AD is more common in individuals over 65 years of age, growing evidence suggests that it may also occur in young adults. Owing to the high cost of treatment, unique epidemiology, and rising frequency globally, it is presently regarded as a contemporary epidemic. According to the 2020 World Alzheimer Report, there are 55 million dementia sufferers worldwide, and by 2050, this number is expected to rise to over 152 million [1]. It is estimated that the illness currently costs the US economy over $1 trillion annually [2].

Cholinergic deficiencies, such as decreased choline acetyl transferase (ChAT) activity and synaptic acetylcholine production, have been linked to cognitive impairments in AD according to the cholinergic hypothesis for AD etiology [3]. These findings were made at the same time as a broader understanding of the cholinergic system's function in memory processing and learning emerged [4]. Acetylcholinesterase (EC 3.1.1.7; AChE) and butyrylcholinesterase (EC 3.1.1.8; BChE) are two forms of cholinesterase enzymes that may break down acetylcholin (Ach) at the neuronal level. AChE is primarily produced by neurons and exhibits dominant activity in healthy brains (80%) [5]. Currently, the implementation of AChE inhibitors to increase cholinergic neurotransmission and decrease the hydrolysis of ACh in the brain is the most effective treatment for AD [6]. Tacrine, donepezil, rivastigmine, and galanthamine are among the AChE inhibitors that have been introduced into the market for the treatment of AD within the last 20 years. Their chemical structures are shown in Figure 1. These medications have significantly improved the care and health of individuals with early-stage AD. AChE inhibitors still raise important scientific and clinical issues, such as their ineffectiveness in individuals with late-stage AD, their potential for peripheral adverse effects, and the rapid development of drug resistance [7]. Therefore, there is a pressing need to

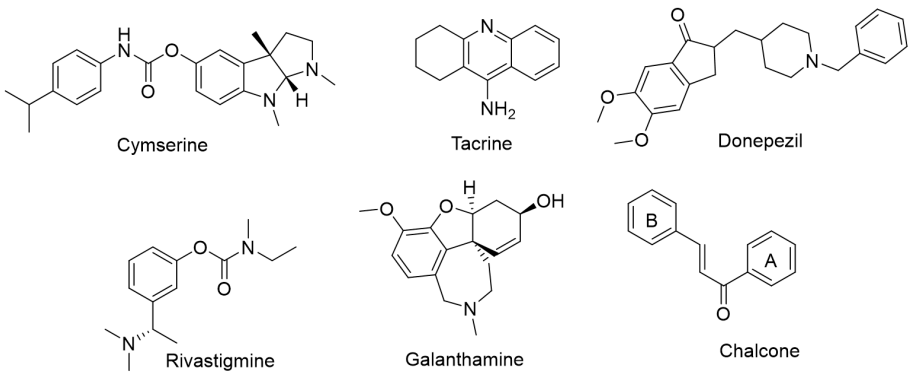

Figure 1 Chemical structures of AChE ligands and chalcone.

find more effective, less hazardous, and potent AChE inhibitors.

Chalcones (1,3-diaryl-2-propen-1-ones) are among the most important natural and synthetic scaffolds. They naturally occur in fruits, vegetables, tea, spices, and meals made from soy and serve as precursors of flavonoids and isoflavonoids [8]. They are structurally open-chain flavonoids with a three-carbon α,β-unsaturated carbonyl system connecting two aromatic rings (A and B), as presented in Figure 1. The Michael acceptor function of chalcone α,β-unsaturated carbonyl functionality interacts with thiols and the sulfhydryl group of cysteine residues at the binding site [9]. This interaction is thought to provide chalcones with diverse biological characteristics [10].

Chalcone-based compounds have gained substantial attention as promising multitarget agents for neurodegenerative disorders such as AD, owing to their demonstrated inhibitory activity against AChE, antioxidant and anti-inflammatory properties, and, in some cases, the ability to inhibit β-amyloid aggregation [11]. Recent structure activity relationship (SAR) studies have shown that substitution patterns on the aromatic rings of the chalcone scaffold for example, electron donating or electron withdrawing groups on ring B, as well as incorporation of additional pharmacophoric moieties (tertiary amines), significantly influence their potency and selectivity toward AChE [12]. Furthermore, hybridization of chalcone with other pharmacophore scaffolds has been reported to further improve inhibitory potency and drug-like properties [13]. In this context, the incorporation of a pyrrole ring into the chalcone framework provides an additional advantage, as pyrrole is a five-membered aromatic heterocycle known to participate in strong π–π stacking, hydrophobic interactions, and hydrogen-bond donor/acceptor interactions within the AChE binding gorge. These features have been shown to enhance ligand affinity toward key residues of the catalytic active site and peripheral anionic site, thereby improving inhibitory activity. Several studies have reported pyrrole-based derivatives as potent AChE inhibitors, supporting the notion that introducing a pyrrolic moiety can significantly strengthen the overall binding profile and pharmacological potential of hybrid molecules [13][14]. Therefore, designing pyrrole–chalcone hybrids represents a rational strategy to exploit the advantageous features of chalcone scaffolds while optimizing interactions within AChE, potentially leading to novel inhibitors with improved efficacy and pharmacokinetic profiles.

Pyrrole contains an *N*-heterocyclic framework that is known to exhibit various biological and medicinal activities [13]. In general, pyrrole derivatives exhibit diverse biological activities, such as antioxidant, antifungal, antituberculosis, anti-inflammatory, analgesic, antidiabetic, and anticancer activities [10]. Furthermore, pyrrole serves as a core structure in many biological compounds, such as chlorophyll, heme, vitamin B12, bile pigments, and alkaloids [15]. Regarding pyrrole-based compounds as potential anti-Alzheimer agents, several studies have reported that triazole derivatives derived from pyrrole exhibit various inhibitory potentials against AChE, with the lowest inhibition concentration values ranging from 5.10±0.40 to 27.10±0.10 μM [10]. The presence of this heterocyclic ring is known to possess intrinsic

biological activity, which can enhance the compound's ability to interact with biological targets, either through non-covalent interactions such as π–π stacking or by increasing lipophilicity and affinity toward enzymes or receptors [16]. Therefore, this study aimed to combine pyrrole and chalcone moieties through Claisen-Schmidt condensation and amidation for further exploration of its potency as an acetylcholinesterase inhibitor.

2. MATERIALS AND METHODS

2.1. Materials

All the chemicals were purchased from commercial vendors (Sigma Aldrich, Merck, and TCI) and used without purification. All solvents employed were analytical grade and used without further purification. The NMR spectra were captured using an Agilent Varian DD2 500 MHz spectrometer (Agilent, USA). Thin-layer chromatography (TLC) was performed using aluminum sheets pre-coated with silica gel GF254 (Merck, Germany) and high-resolution mass spectrometry (HRMS) using an ESI-TOF mass spectrometer (LCT Premier XE, Waters).

2.2. Methods

2.2.1. Synthetic Methods

*2.2.1.1. Synthesis of Compound **2***

A 1.17 g (6 mmol) of ethyl 5-formyl-2,4-dimethyl-1*H*-pyrrole-3-carboxylate and 6 mL of methanol were placed in a 3-neck round-bottom flask equipped with a condenser, connector, and thermometer. NaOH solution (1.20 g in 10 mL of water) was added to the flask, and the reaction mixture was refluxed for 4.5 h. The reaction mixture was cooled to room temperature and transferred to an ice bath (20 mL). The mixture was extracted with 12 mL DCM to remove residual precursors, and the organic phase was washed with 15 mL water three times. The aqueous phases were combined and acidified with 2 M HCl until pH = 2. The precipitation formed was filtered and washed with cold water. The precipitate was left under vacuum for 2 h and dried in an oven at 40 °C for 12 h.

Compound (**2**). Yellow solid, yield: 97%, ^{1}H NMR (500 MHz, DMSO-d_6) δ_H 12.10 (*s*, 1H), 9.59 (*s*, 1H), 2.45 (*s*, 3H), 2.41 (*s*, 3H). ^{13}C NMR (125 MHz, DMSO-d_6) δ_C 178.3, 166.5, 143.3, 134.6, 128.7, 113.8, 14.1, 10.9. HR-ESI-TOF-MS $[M-H]^-$ m/z calc. for $C_8H_8NO_3$: 166.0510, Found: 166.0514.

*2.2.1.2. Synthesis of Compounds **3–6***

5-formyl-2,4-dimethyl-1*H*-pyrrole-3-carboxylic acid (200 mg, 1.1 mmol) was placed in a 10 mL round-bottom flask. Then, 4 mL of methanol and 2 mmol of acetophenone or 4-hydroxyacetophenone were added to the flask, and the mixture was cooled in an ice bath. KOH (671.3 mg, 12 mmol) was added to the cooled mixture, which was then stirred with a magnetic stirrer for 30 min in an ice bath. The mixture was then stirred for 72 h at room temperature. The progress of the reaction was monitored using TLC to determine its completion. After the reaction was completed, the mixture was poured into 10 mL of ice water and acidified with 2 M HCl until the pH = 6. The resulting precipitate was filtered and washed with clean water to remove

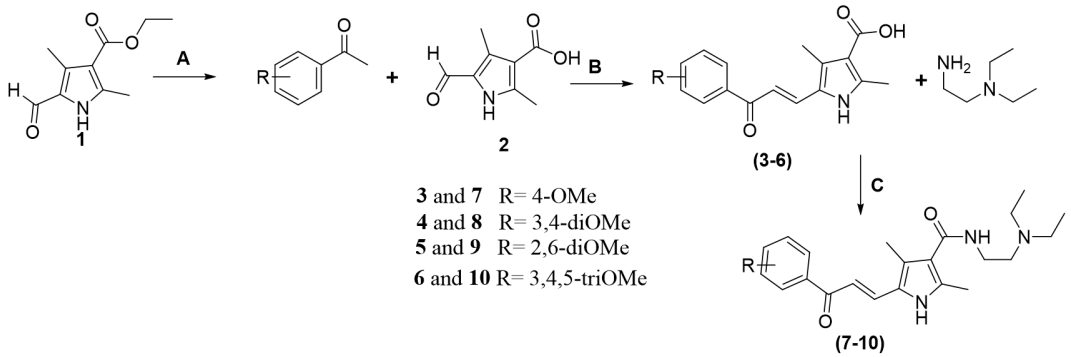

Figure 2. Reagent and conditions: **A**) MeOH, NaOH, reflux, 4.5 h; **B**) MeOH, KOH, 72 h, rt; **C**) THF, CDI, reflux, 3 h.

Tabel 1. *In vitro* acetylcolinesterase inhibitory activity of compounds **1-10**.

Compound	%Inhibition (50 µM)	IC_{50} (µM)
1	No inhibition	-
2	No inhibition	-
3	No inhibition	-
4	No inhibition	-
5	No inhibition	-
6	No inhibition	-
7	54.53	ND
8	77.18	3.19±0.02
9	38.67	ND
10	73.98	2.83±0.51
Galanthamine	97.46	0.53±0.02

the inorganic salts. The precipitate was left under vacuum for 2 h and then left to dry overnight. The purified precipitate was recrystallized from hot methanol.

Compound (**3**). Yellow solid, yield: 62%, ^{1}H NMR (500 MHz, DMSO-d_6) δ_H 11.92 (*s*, 1H), 11.71 (*s*, 1H), 8.02 (*m*, 2H), 7.58 (*d*, *J* = 15.3 Hz, 1H), 7.52 (*d*, *J* = 15.2 Hz, 1H), 7.12 – 7.06 (*m*, 2H), 3.85 (*s*, 3H), 2.49 (*s*, 3H), 2.30 (*s*, 3H). ^{13}C NMR (125 MHz, DMSO-d_6) δ_C 186.9, 166.7, 163.3, 141.1, 131.6, 130.6 (2C), 130.4, 129.2, 125.5, 114.4 (2C), 114.2, 113.6, 56.0, 14.2, 11.5. HR-ESI-TOF-MS $[M-H]^-$ m/z calc. for $C_{17}H_{17}NO_4$: 298.1085, Found: 298.1086.

Compound (**4**). Yellow solid, yield: 60%, ^{1}H NMR (500 MHz, DMSO-d_6) δ_H 11.99 (*s*, 1H), 7.73 (*dd*, *J* = 8.5, 2.0 Hz, 1H), 7.59 (*d*, *J* = 15.1 Hz, 1H), 7.56 – 7.52 (*m*, 2H), 7.02 (*d, J* = 8.5 Hz, 1H), 3.83 (*s*, 3H), 3.82 (*s*, 3H), 2.50 (*s*, 3H), 2.34 (*s*, 3H). ^{13}C NMR (125 MHz, DMSO-d_6) δ_C 186.8, 168.4, 152.9, 149.1, 139.9, 132.0, 130.9, 129.7, 125.0, 122.7, 112.5, 111.2, 110.9, 56.1, 56.0, 39.8, 14.2, 11.6. HR-ESI-TOF-MS $[M+H]^+$ m/z calc. for $C_{18}H_{19}NO_5$: 330.1336, Found: 330.1340.

Compound (**5**). Yellow solid, yield: 27%, ^{1}H NMR (500 MHz, DMSO-d_6) δ_H 11.62 (*s*, 1H), 7.34 (*t*, *J* = 8.4 Hz, 1H), 7.01 (*d*, *J* = 15.0 Hz, 1H), 6.72 (*d*, *J* = 8.5 Hz, 2H), 6.59 (*d*, J = 15.8 Hz, 1H), 3.70 (*d*, *J* = 3.5 Hz, 6H), 2.41 (*s*, 3H), 2.12 (*s*, 3H). ^{13}C NMR (125 MHz, DMSO-d_6) δ_C 193.2, 166.6, 157.2 (2C), 141.5, 131.6, 130.9, 128.9, 124.4, 121.5, 119.1, 113.7, 104.8 (2C), 56.2 (2C), 14.1, 11.4. HR-ESI-TOF-MS $[M+H]^+$ m/z calc. for $C_{18}H_{19}NO_5$: 330.1336, Found: 330.1339.

Compound (**6**). Yellow solid, yield: 77%, ^{1}H NMR (500 MHz, DMSO-d_6) δ_H 11.93 (*s*, 1H), 11.68 (*s*, 1H), 7.61 (*d*, *J* = 15.2 Hz, 1H), 7.44 (*d*, *J* = 15.2 Hz, 1H), 7.31 (*s*, 2H), 3.89 (*s*, 6H), 3.77 (*s*, 3H), 2.51 (*s*, 3H), 2.32 (*s*, 3H). ^{13}C NMR (126 MHz, DMSO-d_6) δ_C 186.8, 168.4, 152.9, 149.1, 139.9, 132.0, 130.9, 129.7, 125.0, 122.7, 112.5, 111.2, 110.9, 56.1, 56.0 (2C), 39.8, 14.2, 11.6. HR-ESI-TOF-MS $[M+H]^+$ m/z calc. for $C_{19}H_{21}NO_6$: 358.1296, Found: 358.1292.

2.2.1.3. Synthesis of Compounds 7–10

A 50 mg (1 equivalent) of the formed chalcone and 2 equivalents of CDI were placed into a carousel tube, followed by the addition of 2 mL of THF. The mixture was refluxed for 3 h. The progress of the reaction was monitored using TLC. Once the chalcone precursor was consumed, 2–5 equivalents of amine were added to the carousel tube. The mixture was stirred at 50 °C overnight and the reaction was monitored by TLC. The reaction mixture was then treated with 20 mL DCM, and excess imidazole and amine were removed by washing with 1 M HCl. The organic phase was dried with anhydrous sodium sulphate, filtered, and the filtrate was evaporated. The precipitate was purified via recrystallization from hot ethyl acetate.

Compound (**7**). Yellow solid, yield: 18%, ^{1}H NMR (500 MHz, DMSO-d_6) δ_H 11.51 (*s*, 1H), 8.02

(*d*, *J* = 8.8 Hz, 2H), 7.56 (*d*, *J* = 15.1 Hz, 1H), 7.48 (*d*, *J* = 15.2 Hz, 1H), 7.24 (*t*, *J* = 5.6 Hz, 1H), 7.09 (*d*, *J* = 8.5 Hz, 2H), 3.86 (*s*, 3H), 3.25 (*d*, *J* = 6.6 Hz, 2H), 2.54 (*q*, *J* = 7.2 Hz, 6H), 2.39 (*s*, 3H), 2.23 (*s*, 3H), 0.98 (*d*, *J* = 7.1 Hz, 6H). ^{13}C NMR (125 MHz, DMSO-d_6) δc 186.8, 165.3, 163.2, 136.0, 135.6, 131.7, 130.9, 130.7 (2C), 130.5, 126.3, 125.1, 119.6, 114.4 (2C), 113.4, 56.0, 52.1, 47.0, 37.2, 13.2, 12.2, 10.8. HR-ESI-TOF-MS $[M+H]^+$ m/z calc. for $C_{23}H_{21}N_3O_3$: 398.2438, Found: 398.2437.

Compound (**8**). Yellow solid, yield: 43%, ^{1}H NMR (500 MHz, DMSO-d_6) δ_H 11.46 (*s*, 1H), 7.71 (*d*, *J* = 8.2 Hz, 1H), 7.55 (*d*, *J* = 15.3 Hz, 1H), 7.53 (*s*, 1H), 7.46 (*d*, *J* = 15.1 Hz, 1H), 7.22 (*s*, 1H), 7.12 (*d*, *J* = 8.4 Hz, 1H), 3.86 (*s*, 3H), 3.84 (*s*, 3H), 3.25 (*d*, J = 6.6 Hz, 2H), 2.51 (*d*, *J* = 7.5 Hz, 8H), 2.39 (*s*, 3H), 2.23 (*s*, 3H), 0.96 (*t*, *J* = 7.1 Hz, 6H). ^{13}C NMR (125 MHz, DMSO-d_6) δ_C 186.9, 165.3, 153.2, 149.2, 136.0, 131.8, 130.6, 126.3, 125.1, 122.7, 119.7, 113.3, 111.3, 111.0, 56.2, 56.0, 52.1, 47.0, 40.0, 37.3, 13.2, 12.3 (2C), 10.8. HR-ESI-TOF-MS $[M-H]^-$ m/z calc. for $C_{24}H_{24}N_3O_4$: 428.2544, Found: 428.2544.

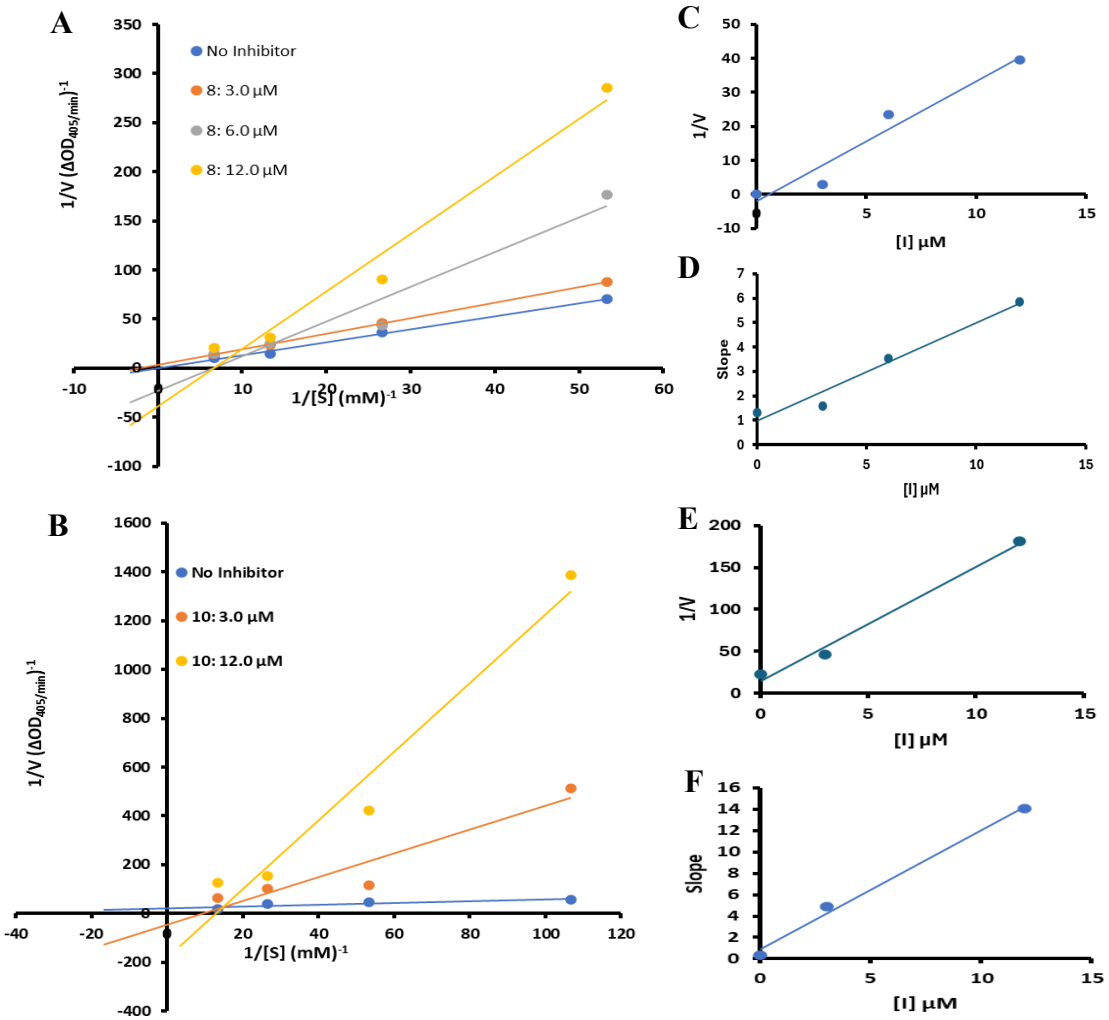

Figure 3. Lineweaver–Burk and secondary plots of acetylcholinesterase inhibition by compounds **8** and **10**. (A, B) Lineweaver–Burk plots for compound **8** (A) and compound **10** (B) showing increasing slopes at inhibitor concentrations of 3.0, 6.0, and 12.0 µM. The lines intersect on the x-axis, indicating unchanged K_m and decreased V_{max}, characteristic of non-competitive inhibition. (C, D) Secondary plots (1/V vs [I] and slope vs [I]) for compound **8**. The linear increases demonstrated consistent slope changes and were used to calculate K_i. (E, F) Secondary plots for compound **10**. Panel e (1/V vs [I]) showed a linear increase in 1/V with increasing [I], while Panel f (slope vs [I]) confirmed a linear relationship that enables *Ki* determination. These results collectively validate the noncompetitive inhibition mechanism.

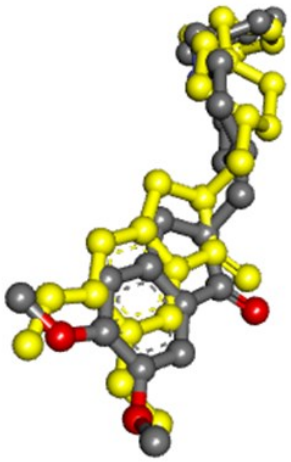

Figure 4. Validation of docking protocol.

Compound (**9**). Yellow solid, yield: 28%, ^{1}H NMR (500 MHz, acetone-d_6) δ_H 10.69 (*s*, 1H), 7.35 (*t, J* = 8.4 Hz, 1H), 7.15 (*d, J* = 15.9 Hz, 1H), 7.06 (*s*, 1H), 6.73 (*d, J* = 8.4 Hz, 2H), 6.53 (*d, J* = 15.9 Hz, 1H), 3.75 (*s*, 6H), 3.39 (*q, J* = 6.0 Hz, 2H), 2.62 (*t, J* = 6.4 Hz, 2H), 2.56 (*q, J* = 7.1 Hz, 4H), 2.46 (*s*, 3H), 2.19 (*s*, 3H), 1.02 (*t*, J = 7.1 Hz, 6H). ^{13}C NMR (125 MHz, acetone -d_6) δ_C 192.4, 164.9, 157.4, 136.0, 135.0, 131.1, 130.2, 125.1, 124.1, 121.1, 119.5, 104.2, 55.3, 51.9, 46.6, 36.9, 12.3, 11.5, 10.0. HR-ESI-TOF-MS $[M+H]^+$ m/z calc. for $C_{24}H_{24}N_3O_4$: 428.2544, Found: 428.2544.

Compound (**10**). Yellow solid, yield: 52%, ^{1}H NMR (500 MHz, DMSO-d_6) δ_H 11.71 (*s*, 1H), 7.58 (*d*, *J* = 15.1 Hz, 1H), 7.44 (*d, J* = 16.8 Hz, 1H), 7.32 (*d*, *J* = 4.4 Hz, 2H), 7.23 (*t*, *J* = 5.6 Hz, 1H), 3.89 (*s*, 6H), 3.76 (*s*, 3H), 3.25 (*q*, *J* = 6.6 Hz, 2H), 2.55 – 2.45 (*m*, 8H), 2.40 (*s*, 3H), 2.24 (*s*, 3H), 0.96 (*t*, *J* = 7.1 Hz, 6H). ^{13}C NMR (126 MHz, DMSO-d_6) δ_C 187.3, 165.2, 153.3 (2C), 142.0, 134.4, 131.4, 126.8, 125.2, 119.8, 113.2, 106.2 (2C), 60.7, 56.7 (2C), 52.1, 47.0 (2C), 39.7, 37.4, 13.3, 12.4 (2C), 10.8. HR-ESI-TOF-MS $[M-H]^-$ m/z calc. for $C_{25}H_{36}N_3O_5$: 458.2649, Found: 458.2647.

2.2.2. Biological Assay

The AChE inhibitory assay was performed using a microplate reader modified from Ellman's colorimetric method as a previous report [17]. Briefly, 25 µL of the sample, 50 µL of 50 mM Tris-HCl buffer A (pH 8.0), 125 µL of 3 mM DTNB in buffer C, and 25 µL of 1.5 mM ATCI in Milli-Q water were added to the wells. Then, 25 µL of 0.3 U/mL enzyme (AChE) in 50 mM Tris-HCl buffer B was added and incubated for 10 min. The reaction was measured at 405 nm using a BIOBASE microplate reader in triplicate. The percentage inhibition at each concentration was calculated by subtracting the observed enzyme activity (%) from 100%. Enzyme activity was calculated as a percentage of the sample rate compared to the negative control. The percentage acetylcholinesterase inhibition was calculated using the following Equation 1.

$$\text{Inhibition (\%)} = 1 - \left(\frac{A_{sample}}{A_{control}}\right) \text{x } 100\% \qquad (1)$$

where A_{sample} is the rate of the reaction of the samples, $A_{control}$ is that of the negative control, and IC_{50} was calculated using percentage inhibition versus concentration. Galantamine was used as a positive control.

2.2.3. Molecular Modeling

The molecular mechanics energy minimization method with the Merck molecular force field (MMFF94) in ChemOffice Professional 15.0 was used to sketch and improve the molecular structure of the synthesized compounds [18][19]. The crystallographic structure of AChE (ID: 1eve) was obtained from the Protein Data Bank (PDB) website (https://www.rcsb.org/) [15]. Molecular docking was carried out using the AutoDock Vina software, with a mode value of 10 and exhaustiveness of 16 for each docked ligand [20]. The AChE-binding site was identified as a 10 Å × 14 Å × 14 Å box at x = 2.023 Å, y = 63.295 Å, and z = 67.062 Å. The docking protocol was validated by redocking the

Table 2. The docking result of the four synthesized compounds (**7-10**), galanthamine, and donepezil.

Compound	Binding Affinity (kcal/mol)
7	-9.0
8	-9.2
9	-9.2
10	-8.9
Galanthamine	-9.6
Donepezil	-10.9

native co-crystallized ligand into the active site, yielding an RMSD value below 2.0 Å, which confirms the reliability and accuracy of the docking procedure [17]. The results were visualized using BIOVIA Discovery Studio Visualizer in 2D interactions [21].

YASARA STRUCTURE version 21.16.17 were used to carry out molecular dynamics (MD) simulations with AMBER14 forcefield [22][23]. The md_run.mcr macros were used in these simulations. The simulation duration was set at 100 ns, and the integration time, also known as the time step, was 2×1.25 fs. Within a single simulation box with 0.9% NaCl, MD simulations were set up to include a temperature of 298 K, pressure of 1 bar, periodic boundaries, solvent density of 0.997, pH of 7.0, Coulomb electrostatics with a 7.86 cutoff, and a temperature of 7.0. To monitor and analyze the behavior of the system, data and trajectories were recorded at regular intervals of 100 ps during the simulations.

2.2.4. ADME Prediction for Drug-likeness

SwissADME was used to study and analyze the ADMET qualities (http://www.swissadme.ch/index.php, retrieved February 26, 2025). These services were selected because they offer relevant pharmacokinetic information for small-molecule medication candidates. After being transformed to SMILES, the structures of pyrrole-fused chalcone amides (**8-10**) were imported into the chosen web services [23].

3. RESULTS AND DISCUSSIONS

3.1. Synthetic Routes Towords Pyrrole-Chalcone Hybrids

Eight novel pyrrole- chalcone hybrids, including four pyrrole-chalcones (**3-6**) and four pyrrole-chalcone amides (**7-10**), were successfully synthesized, as illustrated in Figure 2. In addition, several analytical methods, including ^{1}H- and ^{13}C-NMR and, for novel compounds, high-resolution mass spectrometry (HR-MS), were used to characterize the synthesized pyrrole-chalcones. NMR analysis of the products was carried out and the NMR spectrum for compound **10** (pyrrole-chalcone amides) was described as follows. Two new doublet signals were detected in the ^{1}H NMR spectrum at 7.44 and 7.58 ppm, corresponding to two sp^2 protons in the trans configuration of the chalcone moiety, with a coupling constant of 15.1 Hz. A triplet signal at 7.23 ppm was detected, corresponding to the amide proton. Another new triplet signal was also detected at 0.9 ppm, corresponding to the two sp^3 protons. While the ^{13}C NMR revealed a single signal at 186.6 ppm associated with a conjugated carbonyl. Five signals in the range of 20.5–61.1 ppm were sp^3 carbon belong to aliphatic carbons, and ten signals in the range of 105.82–152.89 ppm were sp^2 carbon belong to aromatic ring.

3.2. Biological Evaluation

Compounds **3-6** and **7-10** were evaluated for their inhibitory activities against acetylcholinesterase. First, all compounds **1-10** were screened at 50 µM against acetylcholinesterase. Pyrrole **1-2** and derivatives **3-6** containing ester and carboxylic acid groups did not inhibit the enzyme. However, the alteration of carboxylic acid (**3-6**) to be the amide groups (**7-10**) exhibited inhibitory activity against acetylcholinesterase, as shown in Table 1. Compounds **7** and **9** inhibited acetylcholinesterase less than 60% inhibition, whereas compounds **8** and

10 demonstrated good inhibitory activity more than 70%. This study indicated that the addition of an amide group to pyrrole-chalcone hybrids enhanced its inhibitory activity against acetylcholinesterase due to increase of its hydrophobicity [24].

Compounds exhibiting inhibition exceeding 70% were subjected to further evaluation to ascertain their IC_{50} values. The findings for the two selected compounds, **8** and **10**, demonstrated significant inhibition of α-acetylcholinesterase, with IC_{50} values of 3.19 and 2.83 µM, respectively, as detailed in Table 1. This study suggested that the presence of two and three methoxy groups at positions 3, 4, and 5 on the phenyl ring that was similar with donepezil structure. Thus, this methoxy group might be essential for sustaining inhibitory activity against acetylcholinesterase at the active site [25].

A kinetic study was conducted to the best inhibitory activity for two compounds (**8** and **10**) to evaluate their inhibition mechanism. The kinetic study result showed that the two selected compounds **8** and **10** exhibited mixed-type inhibition, as presented in Figures 3(A) – 3(B) [26]. Thus, there are two inhibition constant belong to enzyme-inhibitor complex (EI) for K_i value and enzyme-substrate-inhibitor complex (ESI) for K_i' value [27]. The inhibition constant values for compound **8** were recorded at 2.4 µM (K_i) and 0.5 µM (K_i') obtained from slope (Figure 3(D)) and 1/V (Figure 3(C)), respectively. Moreover, compound **10** showed inhibition constant values of 0.8 µM (K_i) and 1.1 µM (K_i') calculated from slope (Figure 3(F)) and 1/V (Figure 3(E)), respectively.

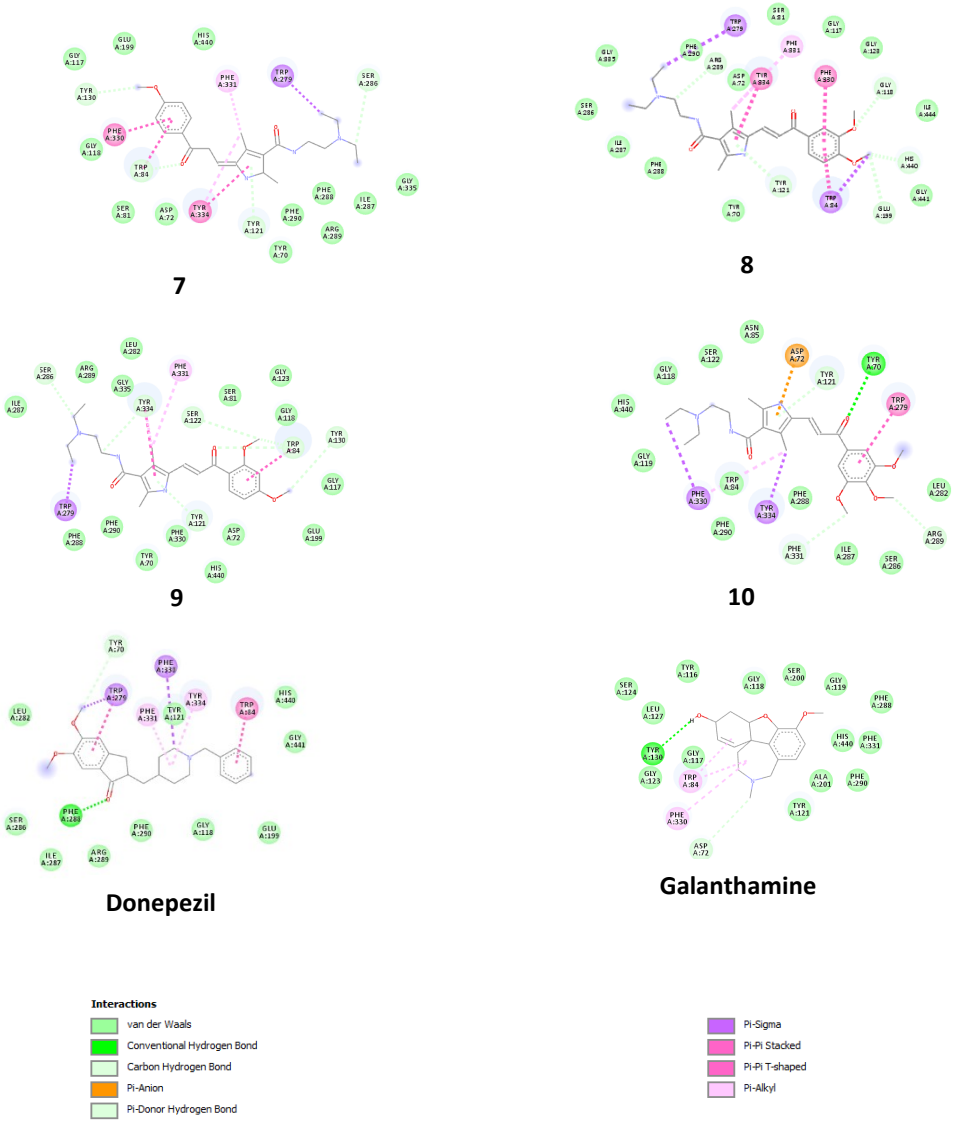

Figure 5. 2D interaction diagrams of Donepezil, Galantamine, and compounds **7–10** with AChE.

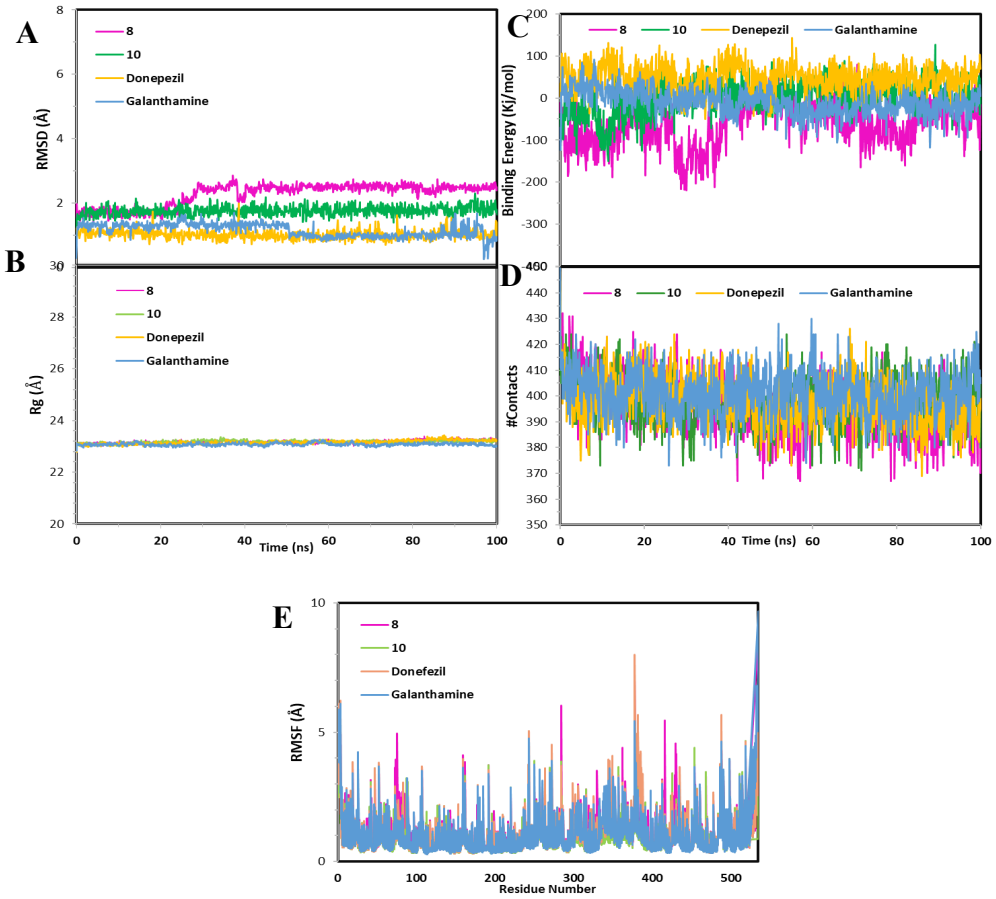

Figure 6. Molecular dynamics (MD) simulation profiles of AChE complexes with compounds **8,10**, donepezil, and galanthamine. (A) RMSD plots showing the backbone stability of AChE-ligand complexes over 100 ns of simulation. (B) Radius of gyration (Rg) plots indicating the overall compactness and structural integrity of the protein in each complex. (C) Binding energy profiles reflecting the consistency and strength of ligand-protein interactions. (D) Number of contacts between ligand and protein residues throughout the simulation, indicating interaction persistence. (E) RMSF plots illustrating residue-level flexibility, particularly at the active site, in response to ligand binding.

Therefore, those compounds could inhibit AChE through two pathways, such as orthosteric binding site (OBS) and allosteric binding site (ABS) [28].

Furthermore, four pyrrole-chalcone amides (**7-10**) were subjected to molecular docking and molecular dynamics simulation to evaluate their potential inhibitory activity against the acetylcholinesterase. Molecular docking was performed on the crystal structure of the AChE in complex with donepezil as the co-crystallized ligand. Validation through the redocking of donepezil, the co-crystallized ligand, into chain A yielded a root mean square deviation (RMSD) of 1.43 Å and a binding affinity of −10.21 kcal mol^{-1} (see Figure 4). The corresponding binding energies are listed in Table 2. The docking results revealed that pyrrole- chalcone amides (**7-10**) exhibited binding affinities (-8.9 to -9.2 kcal/mol), which were slightly lower compared to the reference compounds of galanthamine and donepezil. The best docking conformations of compounds **7-10** and galanthamine within the active site of the cholinesterase enzyme AChE are shown in Figure 5.

3.3. Molecular Docking and Molecular Dynamic

The compounds **7-10** exhibited nearly identical binding energies to AChE, ranging between (-8.9 to -9.2 kcal/mol). The analysis of the best-filtered binding conformations of compounds **7-10** revealed several similarities in the interactions of donepezil with AChE. These include interactions with Trp84,

Phe330, Phe331, and Tyr334, which are crucial residues that form the anionic site that plays a role in stabilizing interactions with the AChE enzyme [29].

The presence of a π-σ interaction at Trp279 with the pyrrole ring in compounds **7-9** contributed significantly to inhibitor binding and substrate access regulation to the catalytic site, enhancing binding affinity. However, the absence of hydrogen bonding in compounds **7-9** resulted in a lower binding energy compared to donepezil. Although compound **10** exhibited hydrogen bonding with Tyr70, its binding energy was not superior to that of compounds **7-9**. Nevertheless, the presence of a π-anion interaction with Asp72 in compound **10** was an important factor in regulating the substrate access to the catalytic site. Interaction analysis revealed that none of the pyrrole-chalcone amides (**7-10**) exhibited interactions at the catalytic site of AChE (Ser200, Glu327, and His440) [29][30].

The molecular docking results show the interaction profiles of standard inhibitors (donepezil and galantamine) and test compounds **7, 8, 9,** and **10** with the active site of AChE. Key interactions include π–π stacking, π–alkyl, π–anion, hydrogen bonding, and van der Waals forces with critical residues such as Trp84, Phe330, Phe331, and Tyr334. Compound **10** displays a more extensive interaction network, like Donepezil, indicating strong binding affinity. Interaction types are color-coded as shown in the legend.

For protein-ligand interactions, the model with the highest AutoDock Vina docking score was used for the MD simulation. This process was performed using the best docking data to examine the dynamics mechanism of molecular interactions at the active site of the enzyme under water conditions. The conformational changes in the protein–ligand complex were examined at every stage, as shown in Figure 6. Molecular dynamics data were analyzed by computing RMSD, binding energy, radius of gyration (Rg), ligand–protein contacts, and RMSF.

The 100 ns MD simulations provided comprehensive insights into the structural stability and binding performance of AChE in complex with compounds **8, 10**, Donepezil, and Galantamine. RMSD plots (Figure 6(A)) revealed that the AChE-compound **10** complex maintained stable backbone deviations (1.5–2.0 Å) throughout the simulation, closely matching the reference ligands. In contrast, compound **8** displayed higher fluctuation (~3.5 Å), suggesting a less stable binding pose. Rg plots (Figure 6(B)) indicated that the compactness of the AChE structure was preserved across all complexes (~23.5 Å), with no significant structural expansion or collapse during the simulation. The binding energy profiles from MM/PBSA analysis (Figure 6 (C)) showed that compound **10** achieved a more negative and consistent binding free energy compared to compound **8,** reflecting stronger and more stable interactions, similar to Donepezil and Galantamine. The number of contacts (Figure 6(D)) further demonstrated that compound **10** sustained a high and steady number of interactions with AChE residues over time, while compound **8** displayed a

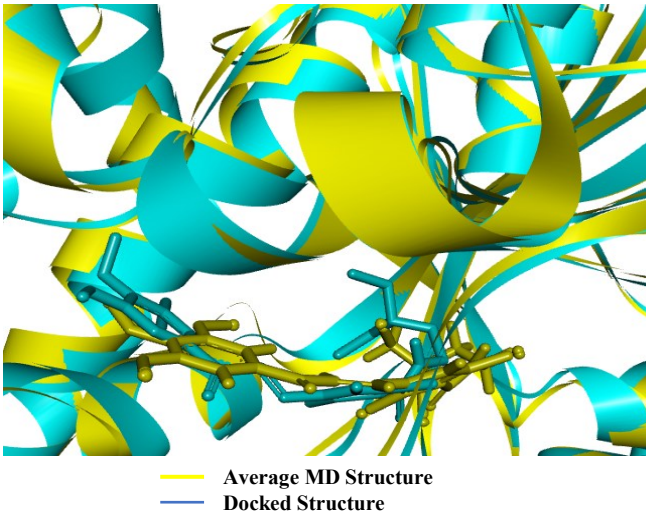

Figure 7. Superimposition of the docked and average MD structure of the AchE-compound **10** complexes.

Table 3. Pharmacokinetics and drug-likeness prediction for compounds **8** and **10**.

Compounds	Lipinski's rule of five and % Absorption						
	Lipinski's rule[a]	TPSA (Å^2)[b]	cLog $P_{o/w}$	GI absorption[c]	Log K_p (cm/s)[d]	BBB permeability[e]	PAINS Alert[f]
8	Yes; 0 violation	83.66	3.46	High	-6.50	No	0
10	Yes; 0 violation	92.82	3.42	High	-6.79	No	0

[a] Molecular weight ≤ 500 Da, hydrogen bond donors ≤ 5, hydrogen bond acceptors ≤ 10, Octanol/water partition coeficient (cLog $P_{o/w}$) ≤ 4.15; [b] Topological polar surface area ≤ 140 Å^2 ; [c] Gastrointestinal absorption ; [d] Skin permeability coeficient ; [e] Blood–brain barrier permeability ; [f] Pan-assay interference compounds alert.

lower and more fluctuating contact profile. More importantly, RMSF analysis (Figure 6(E)) showed that compound **10** effectively stabilized key active-site regions, particularly around Trp84, Phe330, and Tyr334, with reduced per-residue fluctuations compared to compound **8**. This local rigidity is consistent with improved binding persistence and selectivity.

The docked structure (cyan) and the average structure obtained after MD simulation (yellow) are shown superimposed to evaluate the stability and positional retention of compound **10** in the AChE binding site. The ligand maintains a consistent binding orientation, indicating that the compound–enzyme complex remains structurally stable throughout the simulation. Minimal deviation between the two structures suggests strong and persistent interactions during MD.

The superimposition of the docked structure (cyan) and the average MD structure (yellow) of the AChE-compound **10** complexes, as presented in Figure 7, demonstrates minimal deviation in ligand orientation and position. This alignment indicates that compound **10** remains stably bound within the active site throughout the simulation, suggesting strong and sustained interactions with the enzyme. The structural consistency confirms the stability of the complex in an aqueous environment and supports the potential of compound **10** as a promising AChE inhibitor.

3.4. ADME Studies

Compounds **8** and **10**, as presented in Table 3, exhibited high gastrointestinal (GI) absorption and a topological polar surface area (TPSA) ranging from 83.66 and 92.82, which reduced within the optimal range for being considered drug-like [31]. Additionally, both compounds showed negative skin permeability (Log Kp) values ranging from -6.50 to -6.79 cm/s, which were within the acceptable Log Kp range for drug candidates [14]. However, according to SwissADME predictions, compounds **8** and **10** presented challenges in crossing the blood-brain barrier (BBB), as presented in Table 3. One of the major difficulties in drug development for Alzheimer's disease is the inability of molecules to pass through the BBB. More than 98% of all small-molecule drugs fail to penetrate the BBB [32]. These predictions indicated

that compounds **8** and **10** possessed high drug-likeness parameters, including good water solubility, no pan-assay interference compounds (PAINS) warnings, a bioavailability score of 0.55, and a synthetic accessibility score ranging from 2.39 to 4.88.

4. CONCLUSIONS

In conclusion, four new pyrrole-chalcones (**3–6**) and pyrrole-chalcone amides (**7–10**) were successfully synthesized. The IC_{50} values for two compounds (**8** and **10**) were 3.19 and 2.83 μM, respectively, and demonstrated substantial inhibitory activity against acetylcholinesterase (AChE). AChE inhibition was found to be non-competitive in kinetic tests of two pyrrole-chalcone amides, **8** and **10**. Additionally, the results of molecular docking demonstrated that compounds **8** and **10** bind to residues outside the catalytic region through π-sigma, π-anion, and hydrogen-bonding interactions, supporting their non-competitive inhibitory mode. MD simulation results indicated overall system stability and strong ligand binding without significant structural disruption. Furthermore, compounds **8** and **10** are promising drug candidates, as they comply with Lipinski's rule of five according to SwissADME predictions. These findings suggest that pyrrole–chalcone amides hold potential as acetylcholinesterase inhibitors, paving the way for further investigation.

AUTHOR INFORMATION

Corresponding Author

Anita Alni — Organic Chemistry Division, Department of Chemistry, Institut Teknologi Bandung, Bandung-40132 (Indonesia);
orcid.org/0000-0002-2849-1919
Email: alni@itb.ac.id

Authors

Dadan Ridwanuloh — Doctoral Program of Chemistry, Institut Teknologi Bandung, Bandung-40132 (Indonesia); Pharmacy Department, Universitas Buana Perjuangan Karawang, Karawang-41361 (Indonesia);
orcid.org/0000-0002-4781-7339

Ade Danova — Organic Chemistry Division, Department of Chemistry, Institut Teknologi Bandung, Bandung-40132 (Indonesia);
orcid.org/0000-0003-4716-1170

Elvira Hermawati — Organic Chemistry Division, Department of Chemistry, Institut Teknologi Bandung, Bandung-40132 (Indonesia);
orcid.org/0000-0002-5492-3316

Warinthorn Chavasiri — Center of Excellence in Natural Products Chemistry, Department of Chemistry, Chulalongkorn University, Bangkok-10330 (Thailand);
orcid.org/0000-0001-5201-1324

Ihsanawati Ihsanawati — Biochemistry and Biomolecular Engineering Research Division, Department of Chemistry, Institut Teknologi Bandung, Bandung-40132 (Indonesia);
orcid.org/0000-0002-5784-762X

Author Contributions

Conceptualization, Methodology, Formal Analysis, Investigation, and Data Curation, D. R. and A. D.; Software, Validation, and Resources, A. D. and E. H.; Writing – Original Draft Preparation, Visualization, and Funding Acquisition, D. R.; Writing – Review & Editing, D. R., A. D., E. H., W. C., I. I., and A. A.; Supervision, A. D., E. H., I. I., and A. A.; Project Administration, A. D. and E. H.

Conflicts of Interest

The authors declare no conflict of interest. The funding sponsor had no role in the selection of the research topic, study design, data collection, analysis or interpretation, manuscript writing, or in the decision to publish the results.

SUPPORTING INFORMATION

Supplementary data associated with this article can be found in the online version at doi: 10.47352/jmans.2774-3047.375.

ACKNOWLEDGEMENT

The first author acknowledges the doctoral scholarship support from the Center for Higher Education Funding and Assessment, Ministry of Higher Education, Science, and Technology,

Republic of Indonesia, and the Indonesia Endowment Fund for Education (LPDP) through the Beasiswa Pendidikan Indonesia (BPI) program under grant number 202101120924 (0674/J5.2.3/ BPI.06/10/2021). The authors also extend their appreciation to the ITB Integrated Chemistry Laboratory for providing access to NMR spectroscopy and mass spectrometry facilities. Special thanks are given in memory of the late Prof. Yana Maolana Syah for his invaluable guidance, advice, and support throughout the course of this study.

DECLARATION OF GENERATIVE AI

In the preparation of this manuscript, the authors affirm that no generative AI tools were used to generate or analyze any scientific content, data, or results. However, language editing and grammar improvements were conducted with the assistance of generative AI technologies (e.g., ChatGPT by OpenAI) under the full supervision and control of the authors. All content, scientific interpretations, analyses, and conclusions remain entirely the responsibility of the authors. The AI tools were not used to write original scientific content or draw conclusions, and they are not listed as authors or contributors. The use of such tools complies with ethical standards and transparency requirements of the Journal of Multidisciplinary Applied Natural Science.

REFERENCES

[1] P. Mishra, A. Kumar, and G. Panda. (2019). "Anti-Cholinesterase Hybrids As Multi-Target-Directed Ligands Against Alzheimer's Disease (1998–2018)". *Bioorganic & Medicinal Chemistry.* **27** (6): 895-930. 10.1016/j.bmc.2019.01.025.

[2] A. Nandi, N. Counts, J. Bröker, S. Malik, S. Chen, R. Han, J. Klusty, B. Seligman, D. Tortorice, D. Vigo, and D. E. Bloom. (2024). "Cost Of Care For Alzheimer's Disease And Related Dementias In The United States: 2016 To 2060". *npj Aging.* **10** (1): 1-8. 10.1038/s41514-024-00136-6.

[3] P. T. Francis, A. M. Palmer, M. Snape, and G. K. Wilcock. (1999). "The Cholinergic Hypothesis Of Alzheimer's Disease: A Review Of Progress". *Journal of Neurology, Neurosurgery & Psychiatry.* **66** (2): 137-147. 10.1136/jnnp.66.2.137.

[4] R. T. Bartus, R. L. Dean, B. Beer, and A. S. Lippa. (1982). "The Cholinergic Hypothesis Of Geriatric Memory Dysfunction". *Science.* **217** (4558): 408-417. 10.1126/science.7046051.

[5] H. Tago, T. Maeda, P. L. McGeer, and H. Kimura. (1992). "Butyrylcholinesterase-Rich Neurons In Rat Brain Demonstrated By A Sensitive Histochemical Method". *Journal of Comparative Neurology.* **325** (2): 301-312. 10.1002/cne.903250212.

[6] C. Ballard, N. Greig, A. Guillozet-Bongaarts, A. Enz, and S. Darvesh. (2005). "Cholinesterases: Roles In The Brain During Health And Disease". *Current Alzheimer Research.* **2** (3): 307-318. 10.2174/1567205054367838.

[7] A. H. Hasan, S. Shakya, F. H. Hussain, S. Murugesan, S. Chander, M. R. F. Pratama, S. Jamil, B. Das, S. Biswas, and J. Jamalis. (2023). "Design, Synthesis, Anti-Acetylcholinesterase Evaluation And Molecular Modelling Studies Of Novel Coumarin-Chalcone Hybrids". *Journal of Biomolecular Structure and Dynamics.* **41** (21): 11450-11462. 10.1080/07391102.2022.2162583.

[8] T. V. Sreevidya, B. Narayana, and H. S. Yathirajan. (2010). "Synthesis And Characterization Of Some Chalcones And Their Cyclohexenone Derivatives". *Central European Journal of Chemistry.* **8** (1): 174-181. 10.2478/s11532-009-0124-x.

[9] S. Liang, C. Chen, R. Chen, R. Li, W. Chen, G. Jiang, and L. Du. (2022). "Michael Acceptor Molecules In Natural Products And Their Mechanism Of Action". *Frontiers in Pharmacology.* **13** : 1033003. 10.3389/fphar.2022.1033003.

[10] Y. M. Lin, Y. Zhou, M. T. Flavin, L. M. Zhou, W. Nie, and F. C. Chen. (2002). "Chalcones And Flavonoids As Anti-Tuberculosis Agents". *Bioorganic & Medicinal Chemistry.* **10** (8): 2795-2802. 10.1016/S0968-0896(02)00094-9.

[11] G. George, V. P. Koyiparambath, S. Sukumaran, A. S. Nair, L. K. Pappachan, A. G. Al-Sehemi, H. Kim, and B. Mathew. (2022). "Structural Modifications On Chalcone Framework For Developing New Class Of Cholinesterase Inhibitors". *International Journal of Molecular Sciences.* **23** (6): 3121. 10.3390/ijms23063121.

[12] Y. A. Malik, T. A. Awad, M. Abdalla, S. Yagi, H. A. Alhazmi, W. Ahsan, M. Albratty, A. Najmi, S. Muhammad, and A. Khalid. (2022). "Chalcone Scaffolds Exhibiting Acetylcholinesterase Enzyme Inhibition: Mechanistic And Computational Investigations". *Molecules.* **27** (10): 3181. 10.3390/molecules27103181.

[13] S. Khan, T. Iqbal, M. B. Khan, R. Hussain, Y. Khan, and H. W. Darwish. (2024). "Novel Pyrrole Based Triazole Moiety As Therapeutic Hybrid: Synthesis, Characterization And Anti-Alzheimer Potential With Molecular Mechanism Of Protein Ligand Profile". *BMC Chemistry.* **18** (1). 10.1186/s13065-024-01340-x.

[14] S. Sun, T. Shi, Y. Peng, H. Zhang, L. Zhuo, X. Peng, Q. Li, M. Wang, S. Wang, and Z. Wang. (2022). "Discovery Of Pyrrole Derivatives As Acetylcholinesterase-Sparing Butyrylcholinesterase Inhibitor". *Frontiers in Pharmacology.* **13** : 1043397. 10.3389/fphar.2022.1043397.

[15] V. Bhardwaj, D. Gumber, V. Abbot, S. Dhiman, and P. Sharma. (2015). "Pyrrole: A Resourceful Small Molecule In Key Medicinal Hetero-Aromatics". *RSC Advances.* **5** (20): 15233-15266. 10.1039/C4RA15710A.

[16] A. Özdemir, M. D. Altıntop, B. Sever, H. K. Gençer, H. A. Kapkaç, Ö. Atlı, and M. Baysal. (2017). "A New Series Of Pyrrole-Based Chalcones: Synthesis And Evaluation Of Antimicrobial Activity, Cytotoxicity, And Genotoxicity". *Molecules.* **22** (12): 1-16. 10.3390/molecules22122112.

[17] A. Danova, A. C. Christy, I. Musthapa, F. Kurniadewi, W. Chavasiri, D. Mujahidin, R. Roswanda, and E. Hermawati. (2025). "Discovery Of New Acetylcholinesterase Inhibitors Derived From Quinazolinones: Synthesis, In Vitro, And Molecular Docking Study". *Pharmacia.* **72** : 1-10. 10.3897/pharmacia.72.e162676.

[18] T. A. Halgren. (1996). "Merck Molecular Force Field. I. Basis, Form, Scope, Parameterization, And Performance Of MMFF94". *Journal of Computational Chemistry.* **17** (5-6): 490-519. 10.1002/(SICI)1096-987X(199604)17:5/6<490::AID-JCC1>3.0.CO;2-P.

[19] H. Mirzaei, S. Zarbafian, E. Villar, S. Mottarella, D. Beglov, S. Vajda, I. C. Paschalidis, P. Vakili, and D. Kozakov. (2015). "Energy Minimization On Manifolds For Docking Flexible Molecules". *Journal of Chemical Theory and Computation.* **11** (3): 1063-1076. 10.1021/ct500155t.

[20] S. Forli, R. Huey, M. E. Pique, M. F. Sanner, D. S. Goodsell, and A. J. Olson. (2016). "Computational Protein-Ligand Docking And Virtual Drug Screening With The AutoDock Suite". *Nature Protocols.* **11** (5): 905-919. 10.1038/nprot.2016.051.

[21] M. Naufal, E. Hermawati, A. Danova, I. W. Hidayat, and J. Al-Anshori. (2025). "Design, Synthesis, Bioevaluation, And Bioinformatics Study Of 5-Benzylidene Hydantoin Derivatives As Novel Tyrosine Kinase Inhibitors". *ChemistryOpen.* **2500158**. 10.1002/open.202500158.

[22] E. Krieger and G. Vriend. (2015). "New Ways To Boost Molecular Dynamics Simulations". *Journal of Computational Chemistry.* **36** (13): 996-1007. 10.1002/jcc.23899.

[23] Y. Duan, C. Wu, S. Chowdhury, M. C. Lee, G. Xiong, W. Zhang, R. Yang, P. Cieplak, R. Luo, T. Lee, J. Caldwell, J. Wang, and P. Kollman. (2003). "A Point-Charge Force Field For Molecular Mechanics Simulations Of Proteins Based On Condensed-Phase Quantum Mechanical Calculations". *Journal of Computational Chemistry.* **24** (16): 1999-2012. 10.1002/jcc.10349.

[24] L. Kang, X. Gao, H. Liu, X. Men, H. Wu, P. Cui, E. Oldfield, and J. Yan. (2018). "Structure-Activity Relationship Investigation Of Coumarin-Chalcone Hybrids With Diverse Side-Chains As

Acetylcholinesterase And Butyrylcholinesterase Inhibitors". *Molecular Diversity.* **22** (4): 893-906. 10.1007/s11030-018-9839-y.

[25] P. Sawasdee, C. Sabphon, D. Sitthiwongwanit, and U. Kokpol. (2009). "Anticholinesterase Activity Of 7-Methoxyflavones Isolated From Kaempferia Parviflora". *Phytotherapy Research.* **23** (12): 1792-1794. 10.1002/ptr.2858.

[26] A. Sobha, A. Ganapathy, S. Mohan, N. Madhusoodanan, A. D. Babysulochana, K. Alaganandan, and S. B. Somappa. (2024). "Novel Small Molecule-Based Acetylcholinesterase (AChE) Inhibitors: From Biological Perspective To Recent Developments". *European Journal of Medicinal Chemistry Reports.* **12** : 100237. 10.1016/j.ejmcr.2024.100237.

[27] R. Ramadhan and P. Phuwapraisirisan. (2015). "New Arylalkanones From Horsfieldia Macrobotrys, Effective Antidiabetic Agents Concomitantly Inhibiting α-Glucosidase And Free Radicals". *Bioorganic & Medicinal Chemistry Letters.* **25** (20): 4529-4533. 10.1016/j.bmcl.2015.08.069.

[28] A. Danova, K. Pattanapanyasat, K. Hengphasatporn, Y. Shigeta, T. Rungrotmongkol, E. Hermawati, and W. Chavasiri. (2024). "Unlocking E-Arylidene Steroid Derivatives As Promising α-Glucosidase Inhibitors". *ChemistrySelect.* **9** (9): e202303887. 10.1002/slct.202303887.

[29] G. Kryger, I. Silman, and J. L. Sussman. (1999). "Structure Of Acetylcholinesterase Complexed With E2020 (Aricept): Implications For The Design Of New Anti-Alzheimer Drugs". *Structure.* **7** (3): 297-307. 10.1016/S0969-2126(99)80040-9.

[30] A. M. Bondžić, T. D. Lazarević-Pašti, A. R. Leskovac, S. Ž. Petrović, M. B. Čolović, T. N. Parac-Vogt, and G. V. Janjić. (2020). "A New Acetylcholinesterase Allosteric Site Responsible For Binding Voluminous Negatively Charged Molecules—The Role In The Mechanism Of AChE Inhibition". *European Journal of Pharmaceutical Sciences.* **151** : 105376. 10.1016/j.ejps.2020.105376.

[31] B. Kuzu, M. A. Alagoz, Y. Demir, I. Gulcin, S. Burmaoglu, and O. Algul. (2024). "Structure-Based Inhibition Of Acetylcholinesterase And Butyrylcholinesterase With 2-Aryl-6-Carboxamide Benzoxazole Derivatives: Synthesis, Enzymatic Assay, And In Silico Studies". *Molecular Diversity.* 671-693. 10.1007/s11030-024-10828-6.

[32] W. M. Pardridge. (2009). "Alzheimer's Disease Drug Development And The Problem Of The Blood-Brain Barrier". *Alzheimer's & Dementia.* **5** (5): 427-432. 10.1016/j.jalz.2009.06.003.